Supporting information

for

Heterogeneous reaction of sulfur dioxide on mineral dust nanoparticles: from single component to mixed components

Tao Wang[1], Yangyang Liu[1], Yue Deng[1], Hongbo Fu[1], Liwu Zhang[1,2*], Jianmin Chen[1]

[1]Shanghai Key Laboratory of Atmospheric Particle Pollution and Prevention, Department of Environmental Science & Engineering, Fudan University, Shanghai, 200433, Peoples' Republic of China

[2]Shanghai Institute of Pollution Control and Ecological Security, Shanghai, 200092, Peoples' Republic of China

*Corresponding Author: Liwu Zhang (zhanglw@fudan.edu.cn)

Number of pages: 14

Number of figures: 12

Number of tables: 4

Number of equations: 3

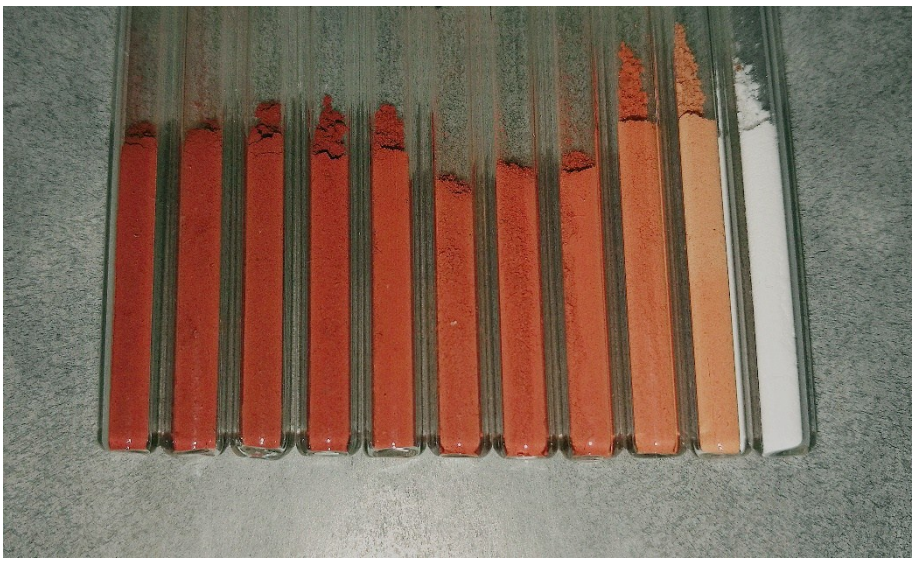

Figure S1. Hematite-alumina mixtures after grinding preparations.

(From left to right, HA-100 to HA-0)

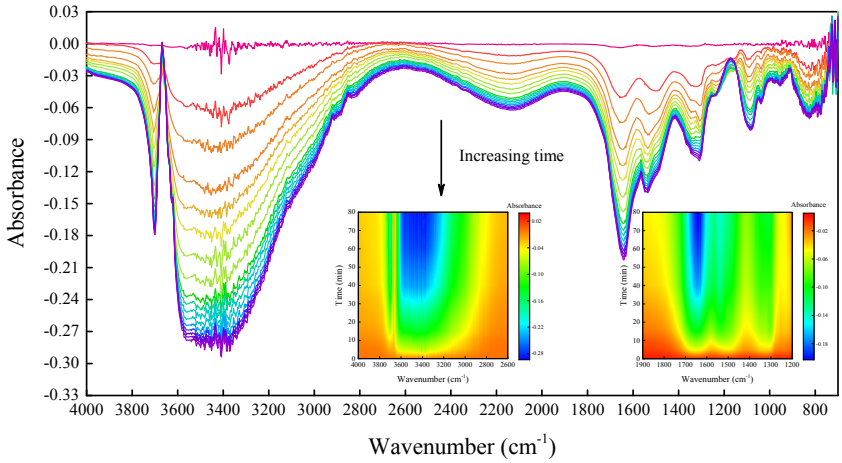

Figure S2. DRIFTS spectra of hematite during pretreatment process.

Before the introduction of SO_2 into the DRIFTS chamber, each sample was pretreated in a stream of high-pure air with a flow of 100 ml·min^{-1} for 60 min to blow off water and impurities on sample surfaces. A background was recorded before the pretreatment, and then a series of spectra were collected every five minutes.

Negative peaks located at 3701 and 1643 cm^{-1}, as well as the broad bands between 3650-2900 cm^{-1} and centered at 2100 cm^{-1} are totally attributed to the vibrations of O-H groups. In detail, the peaks centered at 1643 and 2100 cm^{-1} are both assigned to liquid water,[1-3] whereas the others are characteristics of diverse surface hydroxyl groups.[4-6] Carbonate species formed during sample preparations significantly decreased, as evident by the successive peaks around 1539, 1310 and 1084 cm^{-1}.[7, 8] All the peaks declined over time and then gradually became stable after 45 min. The spectra of all the mixtures are roughly the same. Therefore, 60 min pretreatment was employed in each experiment.

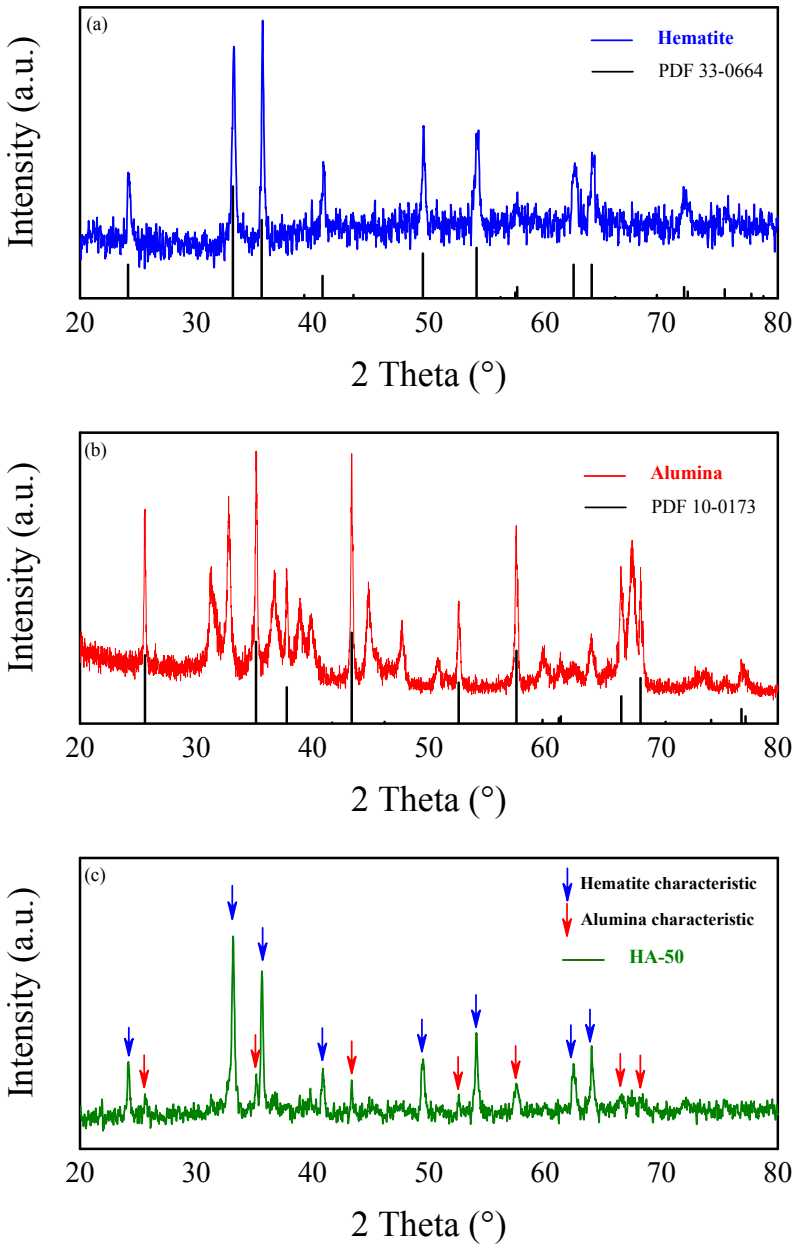

Figure S3. XRD patterns of the (a) laboratory prepared hematite, (b) purchased alumina, and (c) HA-50 mixture. All samples were manually grinded before XRD analysis.

X-ray diffraction (XRD) patterns of the two oxides match well to the standard Joint Committee on Powder Diffraction Standards (JCPDS) Cards of iron oxide (PDF 33-0664) and corundum (PDF 10-0173), respectively.

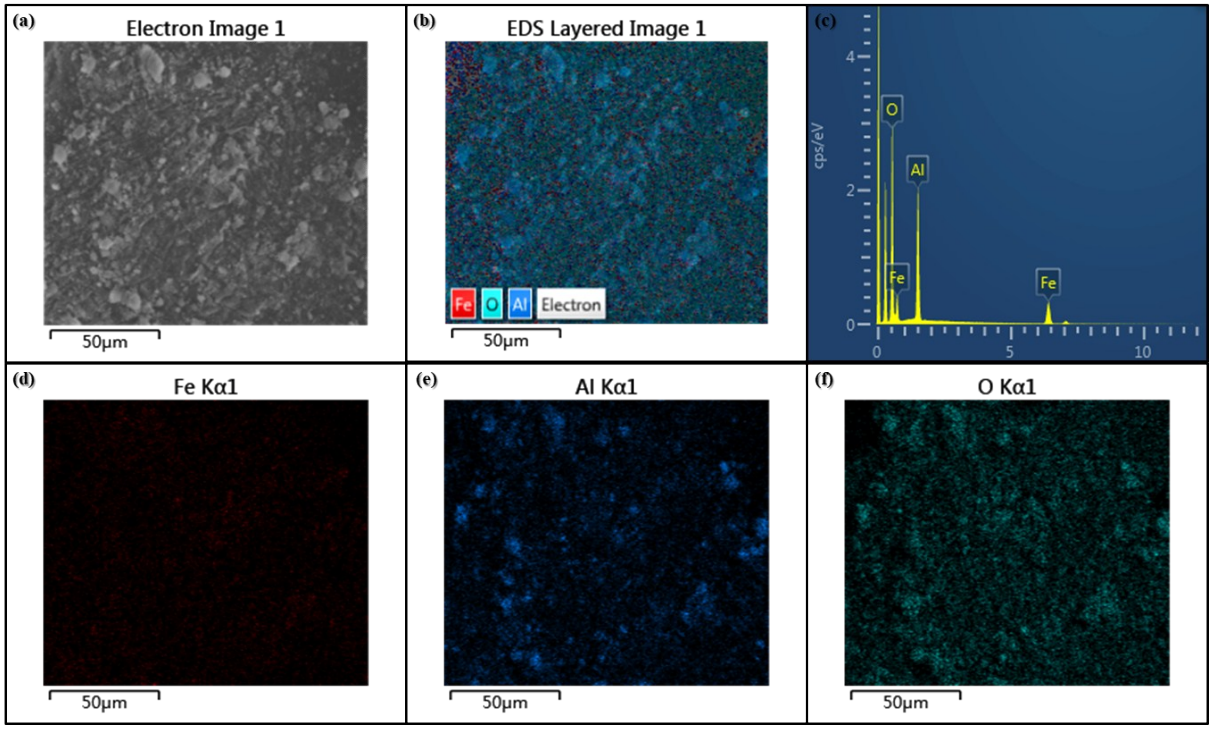

Figure S4. SEM-EDX mapping detection for HA-50 sample: (a) SEM image, (b) element distribution on the selected sample surface, (c) EDX results, as well as detailed element distribution of (d) iron, (e) alumina, and (f) oxygen.

The homogeneous distribution of iron and alumina elements indicates the thorough mixing of the two metal oxides.

Table S1. BET specific surface area (S_{BET}), pore volume and pore size of the hematite-alumina mixtures

Hematite (%)	S_{BET} ($m^2 \cdot g^{-1}$)	Pore volume ($cm^3 \cdot g^{-1}$)	Pore size (nm^2)
0	**46.97**	0.251	21.335
10	**46.19**	0.252	21.705
20	**45.37**	0.249	21.954
30	**43.41**	0.243	22.157
40	**41.65**	0.236	22.387
50	**39.66**	0.226	22.720
60	**37.42**	0.217	23.227
70	**34.60**	0.207	23.984
80	**32.23**	0.199	25.064
90	**29.27**	0.193	26.542
100	**26.23**	0.190	28.491

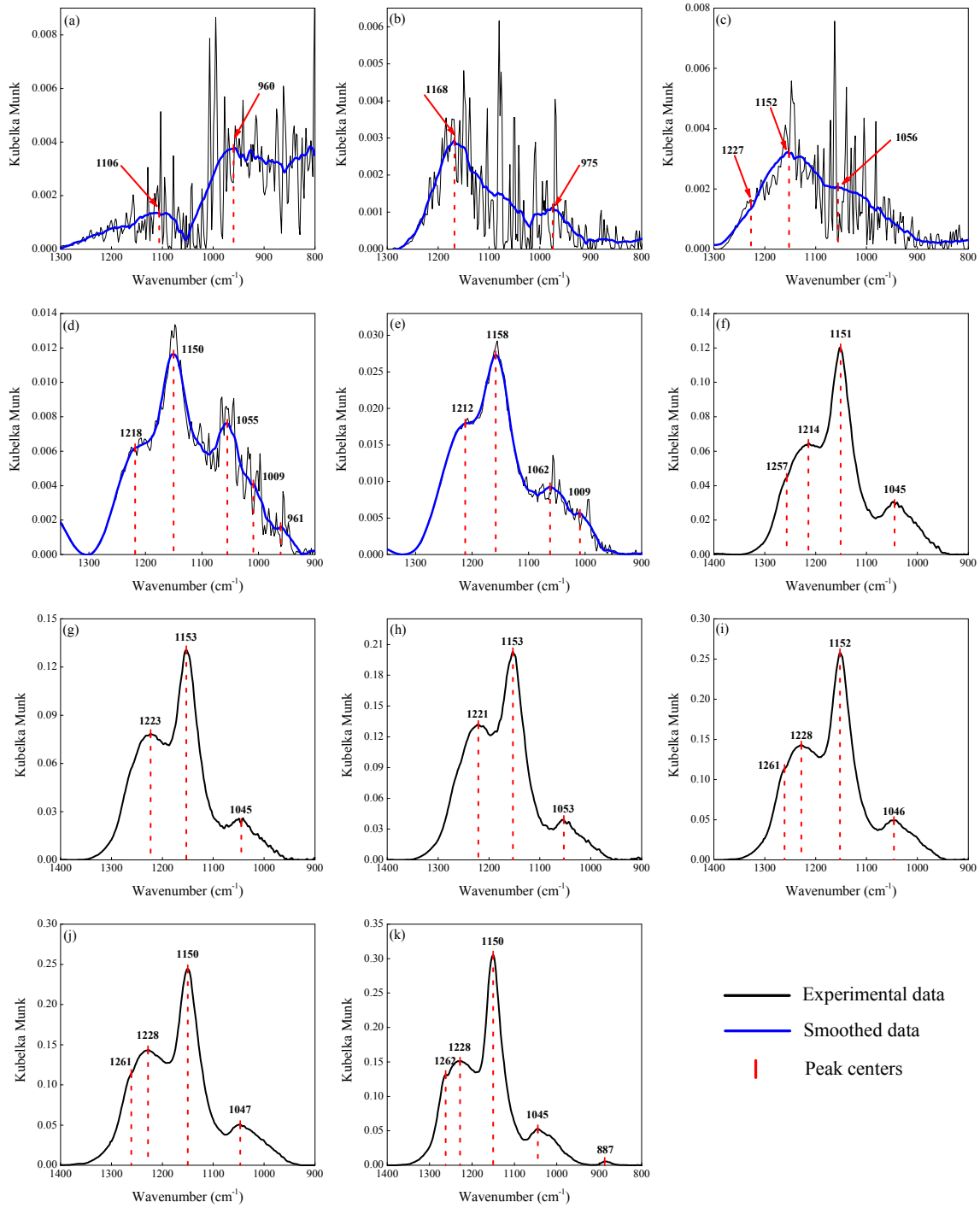

Figure S5. DRIFTS spectra of hematite-alumina mixtures after 60 min exposure to SO_2-containing high-pure air. From a to k: mixtures from HA-0 to HA-100.

Smoothing processes were employed for the spectra of HA-0, HA-10, HA-20, HA-30 and HA-40, owing to the strong lattice oxide absorptions of alumina.[3]

Table S2. Parameters for uptake coefficient calculations

Parameter (unit)		Value
Sulfate formation rate: $d[SO_4^{2-}]/dt$ (ion·s^{-1})		According to reactions
Particle reactive surface area: As (m^2)	A_{BET} (m^2)	S_{BET}×sample mass
	A_{geo} (m^2)	1.96×10^{-5}
Reactant concentration: [SO_2] (molecule·m^{-3})		1.15×10^{20}
Velocity of molecule: v_{SO_2}	Gas constant: R (J·mol^{-1}·K^{-1})	8.314
	Temperature: T (Kelvin)	298
	Molar mass: M_{SO_2} (kg·mol^{-1})	6.4×10^{-2}
	Pi: π (dimensionless)	3.1416

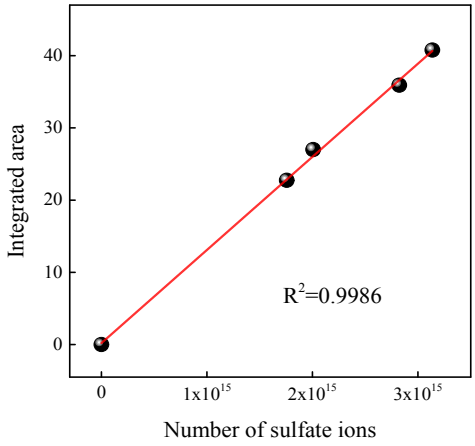

Figure S6. Calibration plot with numbers of SO_4^{2-} versus corresponding integrated areas for sulfate products on hematite.

A conversion is obtained from a calibration plot with the number of SO_4^{2-} analyzed by IC versus the integrated areas for sulfate products on hematite. Ultrapure water (5 ml, specific resistance ≧ 18.2 MΩ cm) containing 1% formaldehyde was used as extraction solvent to prevent oxidation processes. A spectral peak-fitting program using Gaussian-Lorentzian peak fitting was employed to the product spectra, and the integrated areas of sulfate peaks were calculated.

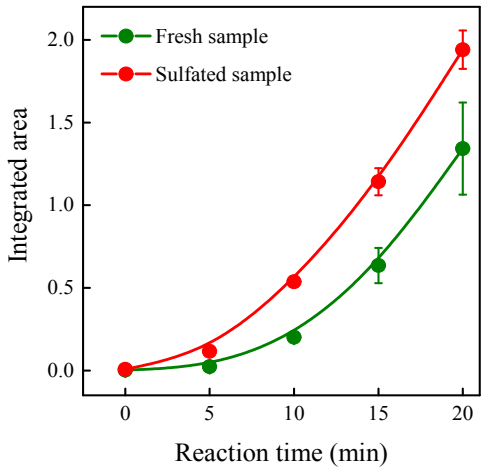

Figure S7. Integrated areas for sulfur-containing products on fresh (green) and sulfated HA-50 (red).

For fresh sample, product formation rate is relatively low in the beginning, resulting probably from the initial diffusion of SO_2 on particle surfaces. The formation rate for sulfated sample (after 20 min in-situ exposure to SO_2) is much higher than that for fresh nanoparticles.

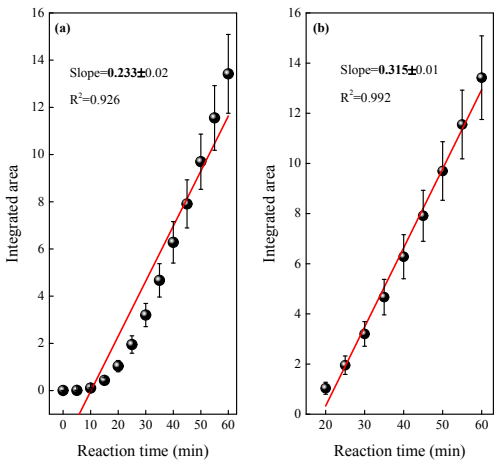

Figure S8. Linear fitting of product integrated areas during different reaction episodes: (a) 0-60 min; (b) 20-60 min. Take HA-50 as an example.

After being introduced to the DRIFTS chamber, some SO_2 molecules diffuse to the nanoparticle surface, resulting in the slow product formation rate in the initial episode (0-20 min). Therefore, for the scatter diagram of product integrated areas as a function of time, the slope and R^2 value of fitted curve become larger if the initial episode is not involved. Uptake coefficients for the whole polluted period (0-60 min) may underestimate the real reactive capacity. To reveal the actual and steady process of SO_2 oxidation, only the latter 40 minutes (20-60 minutes) is involved in the uptake coefficient calculations.

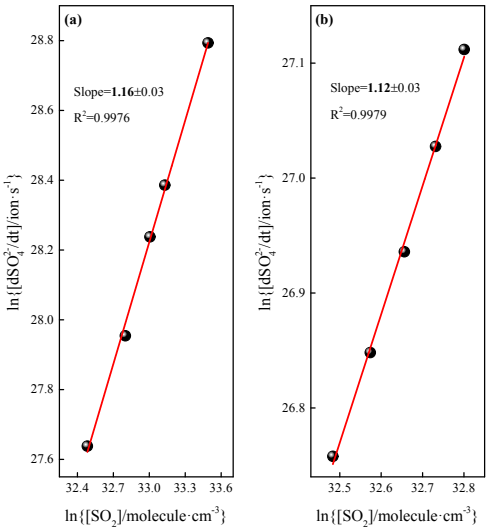

Figure S9. Bilogrithmic plots of the product formation rates versus corresponding SO_2 concentrations for two studied samples: (a) HA-100; (b) HA-50.

In this study, formation rate of sulfur-containing compounds is related to SO_2 concentration, number of active sites on mixture surfaces, and O_2 concentration, which could be shown by **equation S1** based on the law of mass action.[9, 10]

$$d\left[SO_4^{2-}\right]/dt = k[SO_2]^m[Mixture]^n[O_2]^p \qquad Eq.S1$$

Where $\left[SO_4^{2-}\right]$ is the concentration of products, $[SO_2]$ is the concentration of SO_2, $[Mixture]$ is the concentration of active sites on mixture surfaces, $[O_2]$ is the concentration of O_2, m, n, p are the reaction orders of SO_2, active site and O_2, respectively. Oxygen is sufficient for the oxidation processes.[11] No saturation effects on the formation of sulfur-containing products were observed, and thus the $[Mixture]$ is approximately constant.[6] Hence, the product formation rate is largely relative to SO_2 concentration. As reported previously, the reaction order here is determined by double-logarithmic plots of the formation rates versus the SO_2 concentrations based on **equation S2**.[6, 12, 13]

$$\ln\left(d\left[SO_4^{2-}\right]/dt\right) = m\ln[SO_2] + n\ln[Mixture] + p\ln[O_2] + \ln k \qquad Eq.S2$$

The reaction order for HA-100 and HA-50 are 1.16 and 1.12, respectively, both indicating the reaction order of 1 for SO_2. Therefore, the heterogeneous uptake of SO_2 on hematite-alumina mixture can be viewed as pseudo-first-order reaction.

Table S3. Summary of uptake coefficients for the heterogeneous reactions of SO_2 on hematite-alumina mixtures

Hematite (%)	γ_{BET}	γ_{geo}
0	$\mathbf{7.37}\times10^{-13}\pm2.73\times10^{-13}$	$\mathbf{3.42}\times10^{-8}\pm1.44\times10^{-8}$
10	$\mathbf{1.18}\times10^{-12}\pm1.05\times10^{-13}$	$\mathbf{7.56}\times10^{-8}\pm1.61\times10^{-8}$
20	$\mathbf{1.47}\times10^{-12}\pm8.93\times10^{-15}$	$\mathbf{9.12}\times10^{-8}\pm2.58\times10^{-9}$
30	$\mathbf{3.96}\times10^{-12}\pm7.07\times10^{-13}$	$\mathbf{2.49}\times10^{-7}\pm5.36\times10^{-8}$
40	$\mathbf{9.08}\times10^{-12}\pm2.60\times10^{-14}$	$\mathbf{6.57}\times10^{-7}\pm2.51\times10^{-8}$
50	$\mathbf{3.31}\times10^{-11}\pm3.10\times10^{-12}$	$\mathbf{2.30}\times10^{-6}\pm2.58\times10^{-7}$
60	$\mathbf{4.64}\times10^{-11}\pm1.46\times10^{-12}$	$\mathbf{2.80}\times10^{-6}\pm1.12\times10^{-7}$
70	$\mathbf{7.34}\times10^{-11}\pm4.65\times10^{-12}$	$\mathbf{4.29}\times10^{-6}\pm1.60\times10^{-7}$
80	$\mathbf{8.53}\times10^{-11}\pm3.59\times10^{-13}$	$\mathbf{5.15}\times10^{-6}\pm8.74\times10^{-8}$
90	$\mathbf{8.87}\times10^{-11}\pm6.21\times10^{-12}$	$\mathbf{5.20}\times10^{-6}\pm2.66\times10^{-7}$
100	$\mathbf{9.00}\times10^{-11}\pm6.68\times10^{-12}$	$\mathbf{5.68}\times10^{-6}\pm4.14\times10^{-7}$

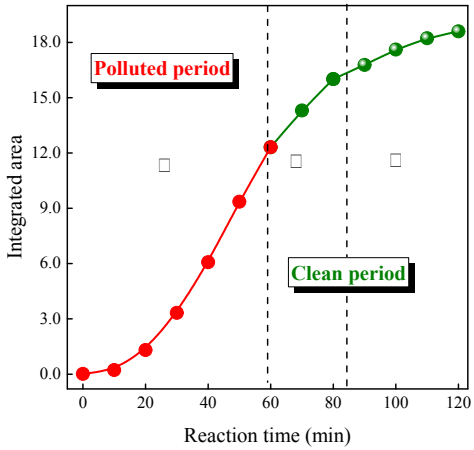

Figure S10. Integrated areas for sulfur-containing products during polluted period (Ⅰ), clean period (Ⅱ), and clean period with the DRIFTS chamber closed (Ⅲ).

The experiment including three steps is aimed at verifying the sources of sulfur-containing products in clean period.

I. Sulfur-containing species were formed on HA-50 along with the introduction of SO_2 in polluted period.

II. SO_2 was cut off and only high-pure air (100 ml·min^{-1}) was introduced for 25 min. The calculated air volume (2500 ml) is 1000 times more than that of the DRIFTS chamber (2.5×10^{-5} m^3). Hence, the chamber was washed for about 1000 times and could be considered clean.[14] The process is mainly aimed at thoroughly flowing away the residual SO_2 in gas supply system and reaction chamber. Prior

research has found the extremely low adsorption capacity of the DRIFTS chamber.[8]

III. Pure air flux was also cut off and then the inlet and the outlet of the chamber were closed. The reaction only proceeded in a closed environment. Formation still occurred during this period.

Therefore, sulfur-containing species formed during clean period originate primarily from the SO_2 physically adsorbed on mixtures in polluted period, rather than the residual SO_2 in gas supply system and/or DRIFTS chamber.

Table S4. Sulfate yields on hematite-alumina mixtures in polluted and clean periods

	Polluted period			Clean period		
Hematite (%)	**Y_{ma} (ion·g^{-1})**	**Y_{st} (ion·g^{-1})**	**Dev**	**Y_{ma} (ion·g^{-1})**	**Y_{st} (ion·g^{-1})**	**Dev**
0	**1.11**×10^{15}±4.82×10^{14}		0.0 %	**7.10**×10^{14}±1.21×10^{15}		0.0 %
10	**1.50**×10^{15}±5.50×10^{12}	**6.68**×10^{15}	-77.6 %	**9.95**×10^{14}±1.38×10^{14}	**1.73**×10^{15}	-42.4 %
20	**1.84**×10^{15}±7.88×10^{13}	**1.22**×10^{16}	-85.0 %	**1.14**×10^{15}±3.90×10^{14}	**2.74**×10^{15}	-58.5 %
30	**4.33**×10^{15}±7.23×10^{14}	**1.78**×10^{16}	-75.7 %	**3.14**×10^{15}±3.38×10^{14}	**3.76**×10^{15}	-16.4 %
40	**8.61**×10^{15}±1.25×10^{13}	**2.34**×10^{16}	-63.1 %	**6.79**×10^{15}±6.25×10^{14}	**4.77**×10^{15}	42.4 %
50	**3.03**×10^{16}±3.21×10^{15}	**2.89**×10^{16}	4.6 %	**1.01**×10^{16}±1.53×10^{15}	**5.79**×10^{15}	74.6 %
60	**4.15**×10^{16}±1.35×10^{15}	**3.45**×10^{16}	20.2 %	**1.04**×10^{16}±1.42×10^{15}	**6.80**×10^{15}	52.5 %
70	**6.15**×10^{16}±4.14×10^{15}	**4.01**×10^{16}	53.5 %	**1.15**×10^{16}±1.01×10^{15}	**7.82**×10^{15}	47.1 %
80	**6.62**×10^{16}±1.30×10^{14}	**4.56**×10^{16}	45.1 %	**1.16**×10^{16}±8.14×10^{14}	**8.83**×10^{15}	31.4 %
90	**6.20**×10^{16}±4.37×10^{15}	**5.12**×10^{16}	21.2 %	**1.19**×10^{16}±1.33×10^{15}	**9.85**×10^{15}	21.2 %
100	**5.68**×10^{16}±4.01×10^{15}		0.0 %	**1.09**×10^{16}±7.26×10^{14}		0.0 %

Deviation (Dev) is calculated in this study based **on equation S3** to present the gaps between Y_{ma} and corresponding Y_{st}.

$$Dev = \frac{(Y_{ma} - Y_{st})}{Y_{st}} \times 100\% \qquad Eq.S3$$

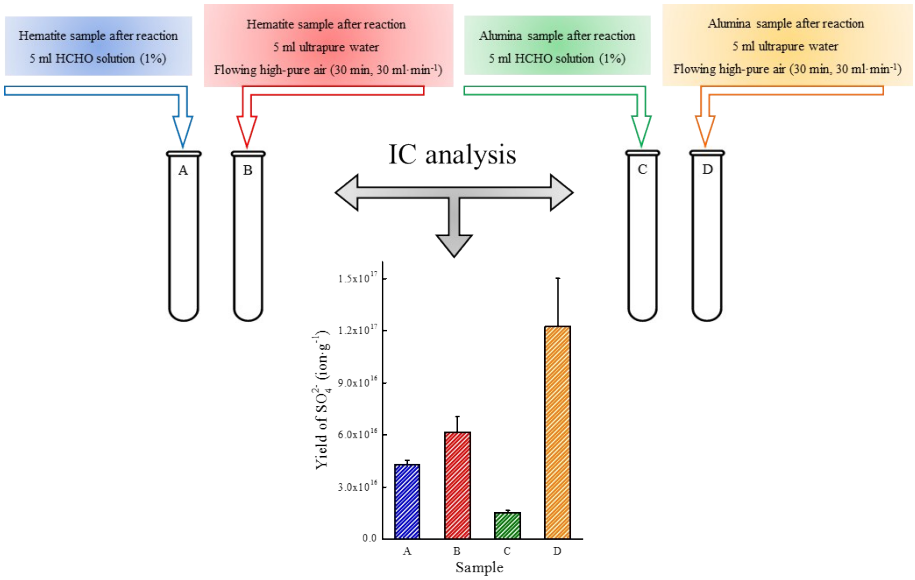

Figure S11. Oxidation of adsorbed SO_2 and sulfite products.

As described in **Figure S10**, a series of experiments were carried out to confirm the physical adsorption of SO_2 on the nanoparticle surface. Each sample was exposed to SO_2 (4.686 ppm) for 50 minutes under dry condition before IC analysis. HCHO solution or high-pure air were introduced to the extraction solutions to prevent or accelerate oxidation processes, respectively. Blank experiments for unreacted samples were considered. The sulfate yields of sample A, B, C and D are denoted as Y_A, Y_B, Y_C and Y_D, respectively.

Y_B is higher than Y_A, and Y_D is higher than Y_C, both suggesting the oxidation of sulfite species. Due to the great capacity of hematite in the heterogeneous oxidation of SO_2 to sulfate products, Y_A is significantly higher than Y_C. Note that, Y_D is extremely higher than Y_B although the integrated area for the total sulfur-containing products on alumina after 60 min SO_2 exposure is much lower than that on hematite **(Figure S4)**. It has been confirmed that physisorbed and chemisorbed SO_2 (surface-coordinated sulfite) are formed after interactions of SO_2 with acid and base sites on α-Al_2O_3 surfaces, respectively.[12, 15, 16] Hence, the gap between Y_C and Y_D is attributed not only to sulfite oxidation, but also the oxidation of large amount of physically adsorbed SO_2 on alumina inner surfaces. As amphoteric metal oxide with relative large S_{BET} and pore volume **(Table S1)**, alumina contains many effective acid sites. As basic metal oxide, hematite contains few acid sites on surfaces, which makes SO_2 physical adsorption difficult.

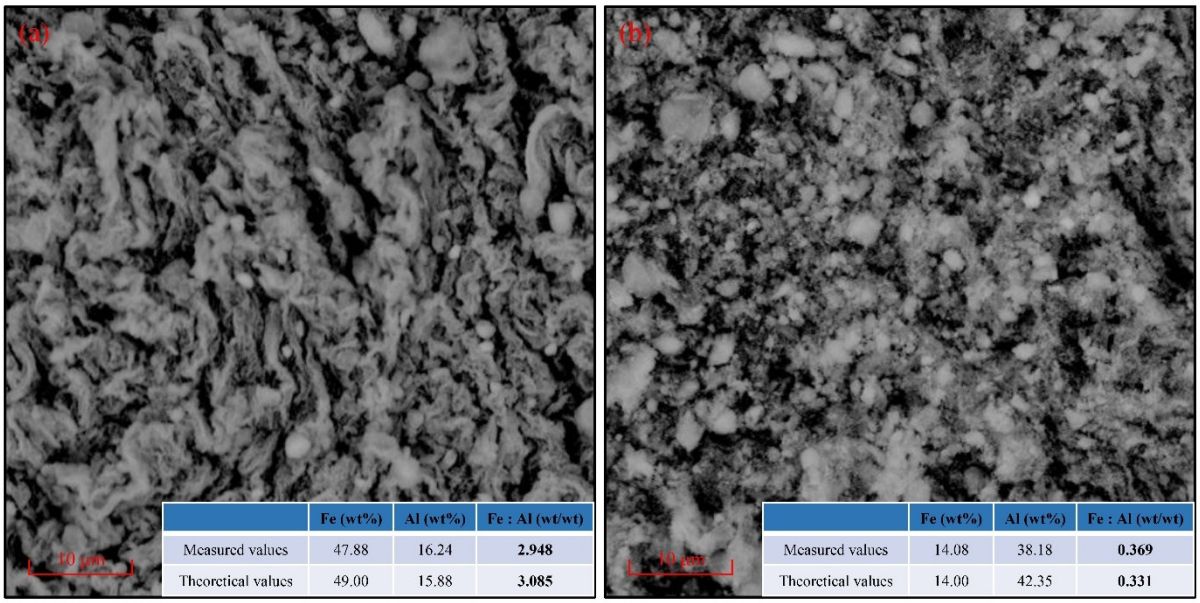

Figure S12. EDX-mapping images of (a) HA-70 and (b) HA-20.

Mapping results from a Phenom XL scanning electron microscope equipped with an energy-dispersive X-ray spectrometer (SEM-EDX) present the mass fractions (%) of Fe and Al in the surface layers of HA-70 and HA-20. There are no significant differences between measured and theoretical values. The hematite proportions of HA-70 and HA-20 calculated by EDX-mapping results are 69.0% and 21.8%, respectively, excluding the possibility of compact surface coating.

References

1 Y. Zhao, Y. Liu, J. Ma, Q. Ma and H. He, *Atmospheric Environment*, 2017, 152, 465-476.
2 H. A. Al-Abadleh and V. H. Grassian, *Langmuir*, 2003, 19, 341-347.
3 Q. Ma, H. He and Y. Liu, *Journal of Environmental Sciences*, 2010, 22, 555-560.
4 C. Deiana, E. Fois, S. Coluccia and G. Martra, *The Journal of Physical Chemistry C*, 2010, 114, 21531-21538.
5 C. E. Nanayakkara, W. A. Larish and V. H. Grassian, *The Journal of Physical Chemistry C*, 2014, 118, 23011-23021.
6 L. D. Kong, X. Zhao, Z. Y. Sun, Y. W. Yang, H. B. Fu, S. C. Zhang, T. T. Cheng, X. Yang, L. Wang and J. M. Chen, *Atmospheric Chemistry and Physics*, 2014, 14, 9451-9467.
7 L. Mino, G. Spoto and A. M. Ferrari, *Journal of Physical Chemistry C*, 2014, 118, 25016-25026.
8 H. Chen, L. Kong, J. Chen, R. Zhang and L. Wang, *Environmental Science & Technology*, 2007, 41, 6484-6490.
9 J. Shang, J. Li and T. Zhu, *Science China Chemistry*, 2010, 53, 2637-2643.
10 J. Li, J. Shang and T. Zhu, *Science China Chemistry*, 2010, 54, 161-166.
11 H. Fu, X. Wang, H. Wu, Y. Yin and J. Chen, *The Journal of Physical Chemistry C*, 2007, 111, 6077-6085.
12 L. W. Wu, S. R. Tong, W. G. Wang and M. F. Ge, *Atmospheric Chemistry and Physics*, 2011, 11, 6593-6605.
13 W. Yang, J. Zhang, Q. Ma, Y. Zhao, Y. Liu and H. He, *Scientific Reports*, 2017, 7, 4550.
14 L. Wu, S. Tong, S. Hou and M. Ge, *Journal of Physical Chemistry A*, 2012, 116, 10390-10396.
15 A. L. Goodman, P. Li, C. R. Usher and V. H. Grassian, *The Journal of Physical Chemistry A*, 2001, 105, 6109-6120.
16 W. Yang, H. He, Q. Ma, J. Ma, Y. Liu, P. Liu and Y. Mu, *Physical Chemistry Chemical Physics*, 2015, 18, 956-964.